

Ultra spin liquid in $\text{Lu}_3\text{Cu}_2\text{Sb}_3\text{O}_{14}$

V. R. Shaginyan,^{1,2,*} A. Z. Msezane,² S. A. Artamonov,¹ G. S. Japaridze,² and Y. S. Leevik³

¹*Petersburg Nuclear Physics Institute, NRC Kurchatov Institute, Gatchina, 188300, Russia*

²*Clark Atlanta University, Atlanta, GA 30314, USA*

³*National Research University Higher School of Economics, St.Petersburg, 194100, Russia*

We analyze recent measurements of C/T , specific heat C divided by temperature T , of recently observed ultra spin liquid. The measurements are carried out in magnetic fields on the triangular lattice compound $\text{Lu}_3\text{Cu}_2\text{Sb}_3\text{O}_{14}$. We show that the obtained heat capacity C_{mag} formed by ultra spin liquid as a function of temperature T versus magnetic field B behaves very similar to the electronic specific heat C_{el} of the HF metal YbRh_2Si_2 and the quantum magnet $\text{ZnCu}_3(\text{OH})_6\text{Cl}_2$. We demonstrate that the effective mass of spinon $M^* \propto C_{\text{mag}}/T$ exhibits the universal scaling coinciding with scaling observed in heavy fermion (HF) metals and in $\text{ZnCu}_3(\text{OH})_6\text{Cl}_2$. Based on these observations we conclude that a strongly correlated spin liquid determines the thermodynamic properties of the ultra spin liquid of $\text{Lu}_3\text{Cu}_2\text{Sb}_3\text{O}_{14}$.

PACS numbers: 75.40.Gb, 71.27.+a, 71.10.Hf

INTRODUCTION

By now, a number of quantum spin liquids (QSL) with various types of ground states are proposed [1–9]. It is expected that QSLs define the thermodynamic, transport and relaxation properties of frustrated magnets and represent the new state of matter formed by strongly correlated Fermi systems [8, 10]. Some of QSLs are formed with fermionic quasiparticles with the effective mass M^* which we call spinons. Spinons carry spin $\sigma = 1/2$ and no charge. At temperature $T = 0$ the Fermi sphere is comprised from spinons with the Fermi momentum p_F . The Fermi sphere can be located near the topological Fermion condensation phase transition (FCQPT) that forms flat bands [10–15]. As a result, the strongly correlated quantum spin liquid (SCQSL) emerges that allows one to describe numerous data related to the thermodynamic, relaxation and transport properties of frustrated magnetic insulators [8, 10, 13, 14, 16–18]. Recent measurements of the specific heat of the triangular lattice compound $\text{Lu}_3\text{Cu}_2\text{Sb}_3\text{O}_{14}$ performed in the presence of magnetic field yield important experimental facts shedding light on the nature of newly discovered ultra spin liquid [9]. It is suggested that the ultra spin liquid is formed by quantum fluctuations. In turn these fluctuations lead to either a large specific heat peak from singlet excitations, or to a degenerate topological singlet ground state [9].

In this Letter we analyze measurements in magnetic fields of the specific heat C_{mag}/T of the ultra spin liquid [9] that forms the thermodynamic properties of $\text{Lu}_3\text{Cu}_2\text{Sb}_3\text{O}_{14}$. We show that obtained $C_{\text{mag}}/T \propto M^*$ as a function of two independent variables magnetic field B and temperature T behaves very similar to the electronic specific heat C_{el}/T of the heavy fermion (HF) metal YbRh_2Si_2 and the specific heat C_{mag}/T of the quantum magnet $\text{ZnCu}_3(\text{OH})_6\text{Cl}_2$. This similarity allows us to conclude that the corresponding QSL is represented by spinons that fill in the Fermi sphere with the Fermi momentum p_F , while the thermodynamic properties of the ultra spin liquid is determined by the strongly correlated quantum spin liquid, rather than by fluctuations. We demonstrate that the effective mass of spinon $M^* \propto C_{\text{mag}}/T$ exhibits scaling similar to that of C_{el}/T and C_{mag}/T .

represented by spinons that fill in the Fermi sphere with the Fermi momentum p_F , while the thermodynamic properties of the ultra spin liquid is determined by the strongly correlated quantum spin liquid, rather than by fluctuations. We demonstrate that the effective mass of spinon $M^* \propto C_{\text{mag}}/T$ exhibits scaling similar to that of C_{el}/T and C_{mag}/T .

UNIVERSAL SCALING BEHAVIOR OF THE ULTRA SPIN LIQUID

The spinons of the triangular lattice compounds occupy a symmetric positions. Consequently, the ground state energy weakly depends on the spins configuration. As a result, the triangular lattice is close to a topologically protected flat branch of the spectrum with zero excitation energy [14, 16, 19–21]. Therefore, the topological FCQPT can be considered as a quantum critical point (QCP) of the $\text{Lu}_3\text{Cu}_2\text{Sb}_3\text{O}_{14}$ ultra spin liquid. We assume that the elementary magnetic excitations, dubbed spinons, defining the thermodynamic properties, carry the effective mass M^* , zero charge and spin $\sigma = 1/2$ and occupy the corresponding Fermi sphere with the Fermi momentum p_F . They form the excitation spectrum typical for HF liquid located near the topological FCQPT and represent HF quasiparticles of deconfined QSL. The ground state energy $E(n)$ is given by the Landau functional that depends on the spinon distribution function $n_\sigma(\mathbf{p})$, with \mathbf{p} being the momentum. Near the FCQPT point, the effective mass M^* is governed by the Landau equation [21, 22]

$$\frac{1}{M^*(T, B)} = \frac{1}{M^*(T=0, B=0)} + \frac{1}{p_F^2} \sum_{\sigma_1} \int \frac{\mathbf{p}_F \mathbf{p}_1}{p_F} F_{\sigma, \sigma_1}(\mathbf{p}_F, \mathbf{p}_1) \frac{\partial \delta n_{\sigma_1}(\mathbf{p}_1)}{\partial p_1} \frac{d\mathbf{p}_1}{(2\pi)^3}. \quad (1)$$

Note that both functional $E(n)$ and Eq. (1) are exact [10, 23]. This fact makes firm ground to construct the theory of HF compounds [10, 14, 21]. Considering that, due to the geometric frustration, QSL in $\text{Lu}_3\text{Cu}_2\text{Sb}_3\text{O}_{14}$ [9] is located near the topological FCQPT, we use the theory of HF compounds to describe SCQSL of $\text{Lu}_3\text{Cu}_2\text{Sb}_3\text{O}_{14}$. This theory allows quantitative analysis of the thermodynamic, relaxation and transport properties of both HF compounds containing QSL and HF metals [8, 10, 13, 14, 16, 21]. As we shall see, the thermodynamic properties of QSL in question coincide with those of SCQSL in the frustrated magnet $\text{ZnCu}_3(\text{OH})_6\text{Cl}_2$ and HF electrons in the HF metal YbRh_2Si_2 .

In Eq. (1) we rewrite the spinon distribution function as $\delta n_\sigma(\mathbf{p}) \equiv n_\sigma(\mathbf{p}, T, B) - n_\sigma(\mathbf{p}, T = 0, B = 0)$. The Landau interaction drives the system to the FCQPT point, where the Fermi surface alters topology of the system so that the effective mass acquires strong temperature and the field dependence [10, 21, 24, 25], as seen from the inset of Fig. 1. Indeed, it is seen from the inset that the effective mass $M^*(T, B) \propto C_{\text{mag}}/T$ strongly depends on both T and B . At the topological FCQPT the term

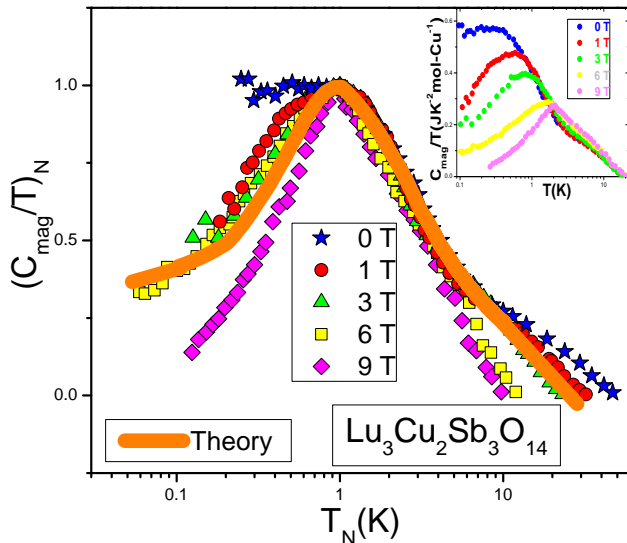


FIG. 1: (color online). The normalized specific heat $(C_{\text{mag}}/T)_N$ of $\text{Lu}_3\text{Cu}_2\text{Sb}_3\text{O}_{14}$ as a function of the normalized temperature T_N measured in the presence of the magnetic field. The normalized specific heat C_{mag}/T is extracted from the measurement of the specific heat of $\text{Lu}_3\text{Cu}_2\text{Sb}_3\text{O}_{14}$ [9] shown in the inset. The solid orange curve corresponds to our theoretical calculations based on Eq. (1). The same curve is depicted in Figs. 2 and 3, demonstrating the universal scaling behavior of the thermodynamic properties of the ultra spin liquid.

$1/M^*(T = 0, B = 0)$ vanishes and Eq. (1) becomes homogeneous and therefore is solved analytically. At $B = 0$, the effective mass depends on T exhibiting the non-Fermi liquid (NFL) behavior [21]

$$M^*(T) \simeq a_T T^{-d}. \quad (2)$$

Here $d = 2/3$ or $d = 1/2$, and can be defined from the corresponding experimental facts [8, 10]. In the case of $\text{Lu}_3\text{Cu}_2\text{Sb}_3\text{O}_{14}$ we have $d = 2/3$. At finite T magnetic field B drives the system to the Landau Fermi liquid (LFL) behavior with

$$M^*(B) \simeq a_B B^{-d}. \quad (3)$$

Here a_T and a_B are fitting parameters.

At finite B and T near the topological FCQPT, the solution of Eq. (1) $M^*(B, T)$ is approximated by a universal interpolating function [21]. The interpolation links the LFL ($M^*(T) \propto \text{const}$) and NFL ($M^*(T) \propto T^{-2/3}$) regions.

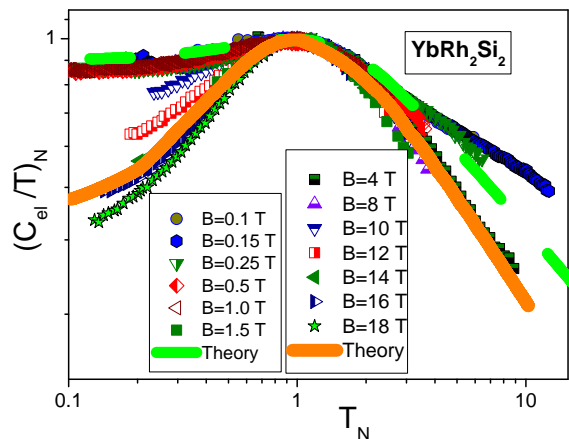


FIG. 2: (color online). The normalized specific heat $(C_{\text{el}}/T)_N = M_N^*$ of YbRh_2Si_2 versus normalized temperature T_N as a function of B at low (the left hand box symbols) and high (the right hand box symbols) magnetic fields, extracted from the measurement of the specific heat on the archetypical HF metal YbRh_2Si_2 [27, 28]. The low-field calculations are depicted by the solid dashed line tracing the scaling behavior of M_N^* . The high-field calculations (solid orange line) are performed for high magnetic fields $B \sim 18$ T when the quasiparticle band becomes fully polarized [17]. At magnetic fields $B \geq 4$ T the specific heat exhibits the same behavior as $(C_{\text{mag}}/T) = M_N^*$ of $\text{Lu}_3\text{Cu}_2\text{Sb}_3\text{O}_{14}$ shown in Fig. 1.

It is seen from the inset of Fig. 1 that C_{mag}/T reaches its maximum value $(C_{\text{mag}}/T)_{\text{max}}(B)$ under the application of magnetic fields at some temperature $T_{\text{max}}(B)$. To reveal the scaling behavior, we introduce the dimensionless normalized specific heat $(C_{\text{mag}}/T)_N$ as a

function of the dimensionless normalized temperature $T_N = T/T_{\max}(B)$ [21]

$$(C_{\text{mag}}/T)_N = \frac{C_{\text{mag}}/T}{(C_{\text{mag}}/T)_{\max}}. \quad (4)$$

As seen from Fig. 1, that $(C_{\text{mag}}/T)_N(T_N)$ as a function of T_N merges into a single curve independent of the applied magnetic field.

In the same way, to construct the interpolating equation and reveal the universal scaling behavior of the effective mass $M^* \propto C_{\text{mag}}/T$, we use the dimensionless normalized effective mass M_N^* and the dimensionless normalized temperature T_N , defined by dividing the effective mass $M^*(T, B)$ by its maximal values, $M_{\max}^*(T, B)$, and temperature T by T_{\max} at which the maximum M_N^* occurs, $T_N = T/T_{\max}$ [21]. Magnetic field B appears in Eq. (1) only in the combination $\mu_B B/k_B T$, thus $k_B T_{\max} \simeq \mu_B B$ where k_B is the Boltzmann constant and μ_B is the Bohr magneton [21, 24]. Thus, $T_{\max} \propto B$ and $T_N \propto T/B$, see e.g. [21, 26]. The normalized effective mass $M_N^* = M^*/M_{\max}^*(T_N \propto T/B) = (C_{\text{mag}}/T)_N$ is given by the interpolating function that approximates the solution of Eq. (1) [21]

$$M_N^*(y) \approx c_0 \frac{1 + c_1 y^2}{1 + c_2 y^8/3}. \quad (5)$$

Here $c_0 = (1 + c_2)/(1 + c_1)$, c_1 and c_2 are fitting parameters, and $y = T/T_{\max} \propto T/B$. It is seen from Eq. (5) that under the application of magnetic field M^* becomes finite and at low temperatures the system exhibits the LFL behavior $C_{\text{mag}}(T)/T \propto M^*(T) \simeq M^*(T=0) + a_1 T^2$. As seen from the inset of Fig. 1, at increasing temperatures $M^* \propto C_{\text{mag}}/T$ increases and enters the crossover region, reaching its maximum $M_{\max}^* \propto (C_{\text{mag}}(T)/T)_{\max}$ at $T = T_{\max}$, with subsequent diminishing given by Eqs. (2) and (5). Equation (5) exhibits the scaling behavior, demonstrating the vivid property of Eq. (1) at the topological FCQPT: the function $M^*(T, B)$ of two variables becomes the function M^* of the single variable $T_N \propto T/B$. We utilize Eq. (5) to outline the universal scaling behavior and clarify our calculations based on Eq. (1).

The scaling of $(C_{\text{mag}}/T)_N = M_N^*$, extracted from $C_{\text{mag}}(T, B)/T$ [9], is reported in Fig. 1. The data for a wide range of B up to 9 T merge well into a single curve. Figure 2 reports the normalized specific heat $(C_{\text{el}}/T)_N = M_N^*$ of YbRh_2Si_2 versus normalized temperature T_N as a function of B . It is seen that at low $T_N \lesssim 0.1$ normalized specific heat $(C_{\text{el}}/T)_N \simeq 0.4$ [17]. This value is determined by the polarization of the heavy electron liquid in magnetic fields $B > 4$ T, and coincides with that of $\chi_N = M_N^*$ obtained on $\text{ZnCu}_3(\text{OH})_6\text{Cl}_2$ and shown in Fig. 3. Results of our calculations are presented by the same solid orange curve in Figs. 1, 2 and 3. Note that at low T_N and at low magnetic field,

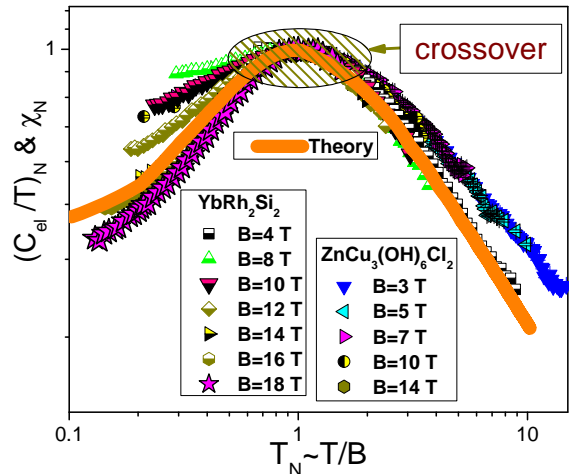


FIG. 3: (color online). Normalized magnetic susceptibility $\chi_N = \chi/\chi_{\max} = M_N^*$ versus normalized temperature $T_N \propto T/B$ as a function of magnetic field shown in the legend. The data are extracted from the measurements of the magnetic susceptibility $\chi(T, B)$ on $\text{ZnCu}_3(\text{OH})_6\text{Cl}_2$ [2]. Normalized data of $(C_{\text{el}}/T)_N = M_N^*$ are obtained from the specific heat C_{el}/T of YbRh_2Si_2 measured in the presence of magnetic field B (the legend) [27]. The solid curve corresponds to the theoretical calculations at $B \simeq 18$ T when the quasiparticle band is fully polarized. The curve represents the universal scaling behavior of M_N^* coinciding with the scaling of the ultra spin liquid which is depicted in Fig. 1. The crossover from the LFL behavior to the NFL one is shown by the arrow.

when the polarization is negligible, $(C_{\text{el}}/T)_N \simeq 0.9$, as seen from Fig. 2. Thus, the behavior of C_{mag}/T reported in Fig. 1 is of universal character, for we observe that $(C_{\text{mag}}/T)_N = M_N^*$ of $\text{Lu}_3\text{Cu}_2\text{Sb}_3\text{O}_{14}$ behaves like $(C_{\text{el}}/T)_N = \chi_N = M_N^*$ shown in Figs. 2 and 3. The data shown in these Figs are extracted from measurements on $\text{ZnCu}_3(\text{OH})_6\text{Cl}_2$ and YbRh_2Si_2 [2, 27, 28]. As a result, the ultra spin liquid can be viewed as SCQSL that exhibits gapless behavior in a magnetic field. We note that the data at magnetic field $B = 0$ and $T_N < 1$ indicate that the ultra spin liquid exhibits the LFL behavior. Otherwise, the spin liquid, being on the ordered side of FCQPT, would have been consumed by phase transition, eliminating the corresponding entropy excess [10, 21]. Therefore, we expect that a stable QSL should be close to the topological FCQPT located on the disordered side of the phase transition.

In Fig. 4 (a), the solid squares denote the values of the maxima $(C_{\text{mag}}/T)_{\max}(B)$, taken from the inset of Fig. 1. In Fig. 4 (a), the corresponding values of $T_{\max}(B)$ are shown versus magnetic field B . It is seen that the agreement between the theory (solid curve) and the experiment is good. At $B = 0$ the arrow shows the

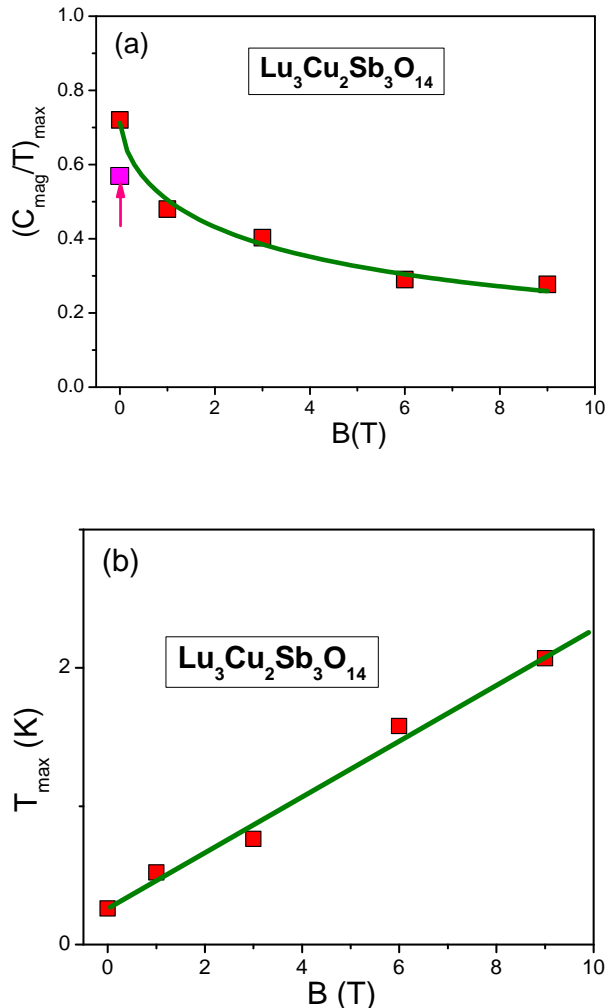


FIG. 4: (color online). (a) The maximums $(C_{\text{mag}}/T)_{\text{max}}$ of C_{mag}/T versus magnetic field B are shown by the solid squares, see the inset, Fig. 1. The solid curve is approximated by $M_{\text{max}}^*(B) \propto B^{-2/3}$, see Eq. (3). The arrow shows the position of $(C_{\text{mag}}/T)_{\text{max}}$ at $B = 0$ with the subtracted impurity Schottky contribution [9]. (b) The temperature $T_{\text{max}}(B)$, at which the maximums of (C_{mag}/T) are located, see Fig. 2 (a). The solid straight line represents the function $T_{\text{max}} \propto B$.

position of the maximum with the subtracted impurity Schottky contribution [9]. We believe that there is no reason to subtract the the impurity Schottky contribution, as it is done in Ref. [9], since both the impurities and the pure crystal holding SCQSL form the integral SCQSL [8]. In Fig. 4 (b), the solid straight line displays the function $T_{\text{max}}(B)$. It is seen that at all temperatures the data are well approximated by the straight line. Note that at $B = 0$ the T_{max} is not clearly discriminated, nonetheless at $B = 0$ and $T \rightarrow 0$ the specific heat C_{mag}/T demonstrates the LFL behavior, as seen from

the inset of Fig. 1. This behavior indicates that SCQSL of $\text{Lu}_3\text{Cu}_2\text{Sb}_3\text{O}_{14}$ is not exactly placed at FCQPT and at $T \rightarrow 0$ the system exhibits the LFL behavior and the absence of a gap. This conclusion concurs with the general properties of the phase diagrams of HF metals and quantum magnets [8, 29]. To clarify the mentioned above properties, one needs to carry out low temperature measurements of both the magnetic susceptibility χ and the thermal transport under the application of magnetic fields. A few remarks are in order here. Recent measurements of the low-temperature thermal conductivity κ have shown that the value of $\kappa(T \rightarrow 0)$ strongly depends on the disorder of quantum magnet and at high disorder $\kappa(T \rightarrow 0) \rightarrow 0$, see e.g. [30, 31]. Such a behavior with $\kappa(T \rightarrow 0) \rightarrow 0$ can signal that QSL is not presented. On the other hand, the thermodynamic properties of some quantum magnets with $\kappa(T \rightarrow 0) \rightarrow 0$ demonstrate the typical behavior of HF metals and one is to suggest that the thermodynamic properties of these magnets are defined by QSL [8, 10, 16]. Thus, we have to assume that there are presented at least the two type of QSL: one of them is presented by QSL with high resistance to the heat transport, that is $\kappa(T \rightarrow 0) \rightarrow 0$, and another is characterized by $\kappa(T \rightarrow 0)$ being finite. In the latter case κ depends on magnetic field resembling the magnetoresistance of HF metals [17, 18]. We speculate that in two dimensional systems, formed by the kagome lattice, spinons can participate in weakly bound states with impurities and that bound states strongly obstruct the heat transport.

Perspective materials, where QSL can be presented, are the Kitaev materials. They can be broadly defined as Mott insulators that exhibit specific exchange interactions and are thought to have unconventional forms of magnetism like QSLs [32]. The experimentally studied examples are Na_2IrO_3 , $\alpha - \text{Li}_2\text{IrO}_3$ and $\alpha - \text{RuCl}_3$ where local moments are aligned in interacting hexagonal layers, see e.g. [8, 33–35]. Measurements of thermal conductivity $\kappa(B)$ under the application of magnetic field B on the insulator $\alpha - \text{RuCl}_3$ have shown that $\kappa(B)$ is finite at $T \rightarrow 0$ when the antiferromagnetic order is suppressed by magnetic field $B = B_c \simeq 7$ T, while $\kappa(B)$ is a growing function at $B > B_c$ [34, 35], since $\kappa(B) \propto (M^*(B))^{-2}$ with $M^*(B)$ is given by Eq. (3) [36]. These observations are in good agreement with the behavior of $\kappa(B)$ of SCQSL, and allows us to suggest that QSL of $\alpha - \text{RuCl}_3$ represents SCQSL, resembling the corresponding behavior of HF metals [8, 10, 18, 36]. A detailed consideration of these items will be published elsewhere.

SCHEMATIC PHASE DIAGRAM OF $\text{Lu}_3\text{Cu}_2\text{Sb}_3\text{O}_{14}$

The schematic phase diagram of $\text{Lu}_3\text{Cu}_2\text{Sb}_3\text{O}_{14}$, based on Eq. (5) and Fig. 1, is depicted in Fig. 5. At $T = 0$ and $B = 0$ the system is located before the topologi-

cal FCQPT, that is on its disordered side. Therefore, at $T = T_0$ the system exhibits the LFL behavior. Both magnetic field B and temperature T play the role of the control parameters, shifting the system from its location close to the topological FCQPT and driving it from the NFL to LFL regions as shown by the vertical and horizontal arrows. At fixed temperatures the increase of B drives the system from the NFL to the LFL region. This

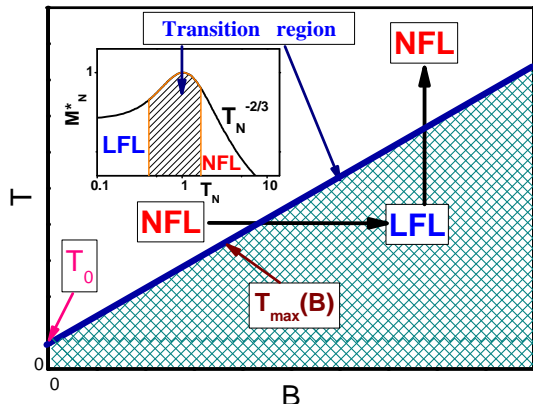


FIG. 5: (color online). Schematic $T - B$ phase diagram of $\text{Lu}_3\text{Cu}_2\text{Sb}_3\text{O}_{14}$ with magnetic field as the control parameter. The vertical and horizontal arrows depicts LFL-NFL transitions at fixed B and T , respectively. The line shown by the arrow represents the crossover region at $T_{\max}(B)$, and displays the function $T_{\max}(B)$. T_0 is the temperature at which the LFL behavior occurs. The inset shows a plot of the normalized effective mass M_N^* versus the normalized temperature T_N . Transition region, at which M^* reaches its maximum M_{\max}^* at $T_N = T/T_{\max} = 1$, is shown by the arrow, see the inset of Fig. 1 as well.

behavior is seen from Fig. 4 (b): Under the application of B , T_{\max} shifts to higher temperatures. Indeed, at $T < T_{\max}$ the system exhibits the LFL behavior [21]. On the contrary, at fixed B and growing temperatures T , the system goes along the vertical arrow from the LFL to NFL region. The inset to Fig. 5 displays the behavior of the normalized effective mass M_N^* versus the normalized temperature $T_N \propto T/B$ that follows from Eq. (5). It is seen that the region $T_N \sim 1$ represents the crossover region between the LFL behavior with almost constant effective mass and the NFL behavior, exhibiting the $T^{-2/3}$ dependence, see Eq. (2) and Fig. 3. It is worthy noting that in the framework of the theory of Fermion condensation it is possible to explain the crossover from the NFL behavior to LFL one under the application of tiny magnetic field [8, 10, 14, 21, 37], while the application of pressure does not change the NFL behavior, see e.g. [38]. Such a behavior observed in the heavy-fermion superconductor $\beta - \text{YbAlB}_4$, representing a strange metal located away from a magnetic instability, is not accompanied by fluctuations [38]. In the same way, one cannot employ

quantum fluctuations to explain the corresponding properties of the phase diagram 5 and the dependencies displayed in Fig. 4 (a,b) [9]. Thus, the general features of the schematic phase diagram 5 demonstrate that the thermodynamic properties of $\text{Lu}_3\text{Cu}_2\text{Sb}_3\text{O}_{14}$ are close to those of the HF metal YbRh_2Si_2 and $\text{ZnCu}_3(\text{OH})_6\text{Cl}_2$ [8, 10, 21]. This confirms our observation that the ultra spin liquid of $\text{Lu}_3\text{Cu}_2\text{Sb}_3\text{O}_{14}$ is represented by SCQSL.

SUMMARY

In summary, we have shown that the ultra spin liquid of $\text{Lu}_3\text{Cu}_2\text{Sb}_3\text{O}_{14}$ can be viewed as a strongly correlated Fermi system whose thermodynamic properties are defined by SCQSL located near FCQPT. Our calculations of the specific heat C_{mag}/T and the constructed phase diagram are in a good agreement with the experimental data. The revealed scaling of C_{mag}/T coincides with that observed in the HF metal YbRh_2Si_2 and quantum magnet $\text{ZnCu}_3(\text{OH})_6\text{Cl}_2$. We have also explained the strong dependence of the maximums of C_{mag}/T on magnetic field B . We remark that such a behavior can hardly be explained within theories based on different kinds of fluctuations. Thus, the ultra spin liquid is well represented by SCQSL, and, therefore, can be well described within the theory of Fermion condensation [8, 10, 14, 21].

ACKNOWLEDGEMENT

We thank V. A. Khodel for fruitful discussions. This work was partly supported by U.S. DOE, Division of Chemical Sciences, Office of Basic Energy Sciences, Office of Energy. This work is partly supported by the RFBR No. 19-02-00237.

* Electronic address: vrshag@thd.pnpi.spb.ru

- [1] P. W. Anderson, Mater. Res. Bull. **8**, 153 (1973).
- [2] J. S. Helton, K. Matan, M. P. Shores, E. A. Nytko, B. M. Bartlett, Y. Qiu, D. G. Nocera, and Y. S. Lee, Phys. Rev. Lett. **104**, 147201 (2010).
- [3] T. H. Han, J. S. Helton, S. Chu, A. Prodi, D. K. Singh, C. Mazzoli, P. Müller, D. G. Nocera, and Y. S. Lee, Phys. Rev. B **83**, 100402(R) (2011).
- [4] L. Balents, Nature **464**, 199 (2010).
- [5] S. Yan, D. A. Huse, and S. R. White, Science **332**, 1173 (2011).
- [6] P. Mendels and F. Bert, J. Phys.: Conference Series **320**, 012004 (2011).
- [7] T. H. Han, J. S. Helton, S. Chu, D. G. Nocera, J. A. Rodriguez-Rivera, C. Broholm, and Y. S. Lee, Nature **492**, 406 (2012).
- [8] V. R. Shaginyan, V. A. Stephanovich, A. Z. Msezane, G. S. Japaridze, J. W. Clark, M. Ya. Amusia, and E. V. Kirichenko, J. Mater. Sci. **55**, 2257 (2020).

- [9] Y. X. Yang, C. Tan, Z. H. Zhu, J. Zhang, Z. F. Ding, Q. Wu, C. S. Chen, T. Shiroka, D. E. MacLaughlin, C. M. Varma, and L. Shu, arXiv: 2102.09271.
- [10] M. Ya. Amusya, V. R. Shaginyan, *Strongly Correlated Fermi Systems: A New State of Matter*, Springer Tracts in Modern Physics Vol. **283** (Springer Nature Switzerland AG, Cham, 2020).
- [11] V. A. Khodel and V. R. Shaginyan, JETP Lett. **51**, 553 (1990).
- [12] G. E. Volovik, JETP Lett. **53**, 222 (1991).
- [13] V. R. Shaginyan, A. Z. Msezane, K. G. Popov, and V. A. Stephanovich, Phys. Rev. Lett. **100**, 096406 (2008).
- [14] M. Ya. Amusia, K. G. Popov, V. R. Shaginyan, and V. A. Stephanovich, *Theory of Heavy-Fermion Compounds*, Springer Series in Solid-State Sciences **182** (Springer, Heidelberg, New York, Dordrecht, London 2015).
- [15] V. A. Khodel, J. W. Clark, and M. V. Zverev Phys. Rev. B **102**, 201108(R) (2020).
- [16] V. R. Shaginyan, A. Z. Msezane, and K. G. Popov, Phys. Rev. B **84**, 060401(R) (2011).
- [17] V. R. Shaginyan, K. G. Popov, V. A. Stephanovich, V. I. Fomichev, and E. V. Kirichenko, Europhys. Lett. **93**, 17008 (2011).
- [18] V. R. Shaginyan, A. Z. Msezane, K. G. Popov, G. S. Japaridze, and V. A. Stephanovich, Europhys. Lett. **97**, 56001 (2012).
- [19] D. Green, L. Santos, and C. Chamon, Phys. Rev. B **82**, 075104 (2010).
- [20] T. T. Heikkilä, N. B. Kopnin, and G. E. Volovik, JETP Lett. **94**, 252 (2011).
- [21] V. R. Shaginyan, M. Ya. Amusia, A. Z. Msezane, and K. G. Popov, Phys. Rep. **492**, 31 (2010).
- [22] L. D. Landau, Sov. Phys. JETP **3**, 920 (1956).
- [23] V. R. Shaginyan, Phys. Lett. A **249**, 237 (1998).
- [24] J. W. Clark, V. A. Khodel, and M. V. Zverev, Phys. Rev. B **71**, 012401 (2005).
- [25] V. A. Khodel, J. W. Clark, and M. V. Zverev, Phys. Rev. B **78**, 075120 (2008).
- [26] V. R. Shaginyan, A. Z. Msezane, J. W. Clark, G. S. Japaridze, Y. S. Leevik, JETP Lett. **112**, 657 (2020).
- [27] P. Gegenwart, Y. Tokiwa, T. Westerkamp, F. Weickert, J. Custers, J. Ferstl, C. Krellner, C. Geibel, P. Kersch, K. H. Müller, and F. Steglich, New J. Phys. **8**, 171 (2006).
- [28] N. Oeschler, S. Hartmann, A. Pikul, C. Krellner, C. Geibel, and F. Steglich, Physica B **403**, 1254 (2008).
- [29] V. R. Shaginyan, A. Z. Msezane, K. G. Popov, G. S. Japaridze, and V. A. Khodel, Europhys. Lett. **106**, 37001 (2014).
- [30] M. Yamashita, Y. Sato, T. Tominaga, Y. Kasahara, S. Kasahara, H. Cui, R. Kato, T. Shibauchi, and Y. Matsuda, Phys. Rev. B **101**, 140407(R) (2020).
- [31] H. Murayama, Y. Sato, T. Taniguchi, R. Kurihara, X. Z. Xing, W. Huang, S. Kasahara, Y. Kasahara, I. Kimchi, M. Yoshida, Y. Iwasa, Y. Mizukami, T. Shibauchi, M. Konczykowski, and Y. Matsuda, Phys. Rev. Res. **2**, 013099 (2020).
- [32] A. Kitaev, Ann. Phys. (Leipzig) **321**, 2 (2006).
- [33] L. Savary and L. Balents, Rep. Prog. Phys. **80**, 016502 (2017).
- [34] Y. Kasahara, T. Ohnishi, Y. Mizukami, O. Tanaka, Sixiao Ma, K. Sugii, N. Kurita, H. Tanaka, J. Nasu, Y. Motome, T. Shibauchi, and Y. Matsuda, Nature **559**, 227 (2018).
- [35] P. Czajka, T. Gao, M. Hirschberger, P. Lampen-Kelley, A. Banerjee, J. Yan, D. G. Mandrus, S. E. Nagler, and N. P. Ong, Nat. Phys. **17**, 915 (2021).
- [36] V. R. Shaginyan, A. Z. Msezane, K. G. Popov, G. S. Japaridze, and V. A. Khodel, Europhys. Lett. **103**, 67006 (2013).
- [37] V. R. Shaginyan, A. Z. Msezane, K. G. Popov, J. W. Clark, V. A. Khodel, and M. V. Zverev, Phys. Rev. B **93**, 205126 (2016).
- [38] T. Tomita, K. Kuga, Y. Uwatoko, P. Coleman, S. Nakatsuji, Science **349**, 506 (2015).